Research Article | Vol. 31, No. 10 / 8 May 2023 / Optics Express 15779
Optics EXPRESS

Native defect clustering-induced carrier localization centers leading to a reduction of performance in $Ga_{0.70}In_{0.30}N$/GaN quantum wells

DONG-PYO HAN,[1,2,*] JIWON KIM,[2] DONG-SOO SHIN,[2] AND JONG-IN SHIM[2]

[1]BK21 FOUR ERICA-ACE Center, Hanyang University, Ansan, Gyeonggi 15588, Republic of Korea
[2]Department of Photonics and Nanoelectronics, Hanyang University, Ansan, Gyeonggi 15588, Republic of Korea
[*]dphan@hanyang.ac.kr

Abstract: In this study, we aimed to better understand the mechanism for creating carrier localization centers (CLCs) in $Ga_{0.70}In_{0.30}N$/GaN quantum wells (QWs) and examine their impacts on device performance. Particularly, we focused on the incorporation of native defects into the QWs as a main cause of the mechanism behind the CLC creation. For this purpose, we prepared two GaInN-based LED samples with and without pre-trimethylindium (TMIn) flow-treated QWs. Here, the QWs were subjected to a pre-TMIn flow treatment to control the incorporation of defects/impurities in the QWs. In an effort to investigate how the pre-TMIn flow treatment affects the incorporation of native defects into the QWs, we employed steady-state photo-capacitance and photo-assisted capacitance-voltage measurements, and acquired high-resolution micro-charge-coupled device images. The experimental results showed that CLC creation in the QWs during growth is closely related to the native defects, most likely V_N-related defects/complexes, since they have a strong affinity to In atoms and the nature of clustering. Moreover, the CLC creation is fatal to the performance of the yellow-red QWs since they simultaneously increase the non-radiative recombination rate, decrease the radiative recombination rate, and increase operating voltage—unlike blue QWs.

1. Introduction

Recently, the demand for semiconductor optoelectronic devices has rapidly increased owing to their smaller size, longer lifetime span, and higher efficiency compared to conventional devices [1,2]. Among them, three primary color semiconductor light-emitters are currently attracting great attention as potential light sources for next-generation displays and applications [3,4]. After a high-quality and a p-type GaN layers were successfully demonstrated by Akasaki and Amano, AlGaInN-based semiconductor light-emitters employing a 2-D quantum-well (QW) active layer have become a dominant light source in blue and green spectral regions [5,6]. As a result, they are being applied as general white light sources and visible light sources for various applications.

For GaInN/GaN QWs, emission wavelengths can be simply tuned by adjusting the indium (In) composition therein (i.e., the emission wavelength shifts toward longer wavelengths as the In composition increases) [7,8]. However, a critical challenge for GaInN/GaN QWs involves reductions in internal quantum efficiency (IQE) as the In composition increases from blue to yellow-red emission wavelengths [9–12]. Numerically, the IQE of blue light-emitting devices (LEDs) reportedly exceeds 90%. In contrast, yellow-red LEDs demonstrate IQEs lower than 10% [9,13,14]. Overcoming this challenge will facilitate the development of next-generation applications and displays which require high color rendering indices. Multiple past studies have attempted to identify potential root-causes of this challenge, including the quantum-confined Stark effect (QCSE) caused by mechanical strain, crystal imperfections due to misfits/dislocations,

#486721 https://doi.org/10.1364/OE.486721
Journal © 2023 Received 31 Jan 2023; revised 6 Apr 2023; accepted 13 Apr 2023; published 26 Apr 2023

Optics EXPRESS

excess defects/impurities incorporation in QWs, and random alloy fluctuations due to phase separation during metalorganic vapor phase epitaxy (MOVPE) growth [9–14]. Based on the studies, various approaches were carried out to overcome the challenge, including hybrid-structure of QWs [15], non-polar/semi-polar growth [16], an AlGaN capping layer [17], an AlN buffer layer [18], In-rich dots [19], a 3–D nano rod structure [20], and a tunnel junction structure [21]. Typically, the QCSE decreases radiative recombination rate, whereas the crystal imperfections and defects/impurities incorporation in the QWs increase non-radiative Shockley-Read-Hall (SRH) recombination rate. Notably, recent studies have reported that the carrier localization, followed by the random alloy fluctuation, is fatal to the performance of yellow-red QWs since it drastically decreases the radiative recombination probability [22–24]. These processes are considerably different than for blue QWs where the carrier localization prevents carrier capture at non-radiative recombination centers (NRCs), thereby increasing the IQE [25,26]. That is to say, the carrier localization is believed to play a key role in reducing the IQE in yellow-red QWs. Thus, if we are to overcome the challenge, understanding the mechanism for creating carrier localization centers (CLCs) and examining their impact on the QWs performance are believed to be of prime importance.

In this study, we aimed to better understand how CLCs are created during MOVPE growth and examine their impacts on yellow-red GaInN/GaN QW performance. Notably, we studied the mechanisms for creating CLCs in the QWs focusing on incorporation of defects/impurities into the QWs. For this purpose, we prepared two $Ga_{0.70}In_{0.30}N$/GaN-based LED samples with and without pre-trimethylindium (TMIn) flow-treated QWs. Here, the QWs were subjected to a pre-TMIn flow treatment to control incorporation of defects/impurities in the QWs [27]. In an effort to investigate how the pre-TMIn flow treatment affects the incorporation of defects/impurities in the QWs, we employed steady-state photo-capacitance (SSPC) and photo-assisted capacitance-voltage (PACV) measurements. Furthermore, in an effort to investigate how the incorporated defects/impurities in the QWs affect the CLC creation, we acquired high-resolution micro-charge-coupled device (μ-CCD) images. Considering the experimental results, we elucidated the mechanisms for creating CLCs with native defects incorporated in the QWs. We subsequently discussed the role of the CLCs in the QW performance by comparing the electrical/optical characteristics of the samples.

2. Sample preparation

To prepare the samples, we fabricated two GaInN/GaN-based LEDs on a flat *c*-sapphire substrate using the MOVPE (EMC, Taiyo Nippon Sanso Co., Japan) equipped with 2-inch susceptors. The detailed structures of the samples are as follows. For sample A, the structure was conventional and consisted of (from the substrate), a 30 nm thick low-temperature GaN buffer layer grown at 480°C, a 3 μm thick un-doped GaN template layer grown at 1070°C, a 2 μm thick Si-doped n-type GaN layer grown at 1070°C, and a 1 μm thick n-type $Al_{0.03}Ga_{0.97}N$ layer grown at 1090°C. Here, the n-$Al_{0.03}Ga_{0.97}N$ layer was employed to decrease the resistance of the device [28,29]. Fifteen pairs of $Ga_{0.97}In_{0.03}N$ (1.5 nm)/GaN (1.5 nm) superlattices grown at 860°C as an underlying layer (UL) and five pairs of $Ga_{0.70}In_{0.30}N$ (3 nm)/GaN (12 nm) QWs layer grown at 640°C/780°C as an active layer were sequentially grown on the n-type $Al_{0.03}Ga_{0.97}N$ layer. Note that the barriers were lightly Si-doped, whereas the wells were intentionally un-doped. Following this, an 80 nm thick Mg-doped p-type $Al_{0.08}Ga_{0.92}N$ layer as an electron blocking layer (EBL), a 150 nm thick Mg-doped p-type GaN layer, and a 20 nm thick heavily Mg-doped p^+-GaN as a contact layer were sequentially grown at 1120°C on the active layer. After removing the sample from the MOVPE reactor, the sample was etched by inductively coupled plasma (ICP) etching system (NE-550EX, ULVAC Co., Japan) using a mixed gas of Cl_2 and Ar to expose the n-type $Al_{0.03}Ga_{0.97}N$ GaN layer, a 60 nm thick indium-tin-oxide layer was then deposited by a radio frequency sputter system (CFS-4EP, Shibaura Mechatronics Co., Japan) on the p^+-GaN contact

Optics EXPRESS

layer as a current spreading/injection layer. After that, the sample was fabricated on a flip-chip device with lateral Cr/Ni/Au electrodes (chip size: 300×300 μm^2) and packaged as surface mount devices. The fabrication of sample B was based on the structure of sample A, which employed five pairs of pre-TMIn flow-treated QWs. That is, samples B and A feature identical structures, with the exception of the five pairs of pre-TMIn flow-treated QWs. For the pre-TMIn flow treatment of the QWs, we followed the sequence illustrated in Fig. 1 consisting of 15 s of stabilization to ensure the gas/temperature change, residual atom removal in the MOVPE reactor, and 15 s of TMIn flow (50 sccm) before QW growth. Note that no gas besides the N_2 carrier gas was supplied during the pre-TMIn flow treatment of the QWs. This avoids unwanted layer/dot growth between the wells and the barriers, which lets us focus on the atomic reaction, rather than the structural effects. To ensure that the samples were grown as intended, we investigated the interfacial and structural properties of the QWs by measuring high-resolution $2\theta-\omega$ X-ray diffraction (XRD) scan spectra (Ultima IV, Rigaku Co., Japan) before the ICP etching. As shown in Fig. 2, the 0th-order and other high-order satellite peaks toward the UL of the XRD scan data were separated almost identically [29]. Indeed, the pre-TMIn flow treatment of the QWs had a negligible effect on the interfacial and structural properties of the QWs, i.e., no layers and/or dots were additionally grown during the pre-TMIn flow-treatment, as we intended [30].

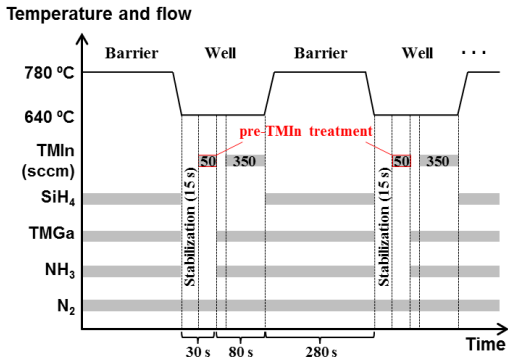

Fig. 1. Growth sequences for the pre-TMIn flow treatment of the QWs in sample B.

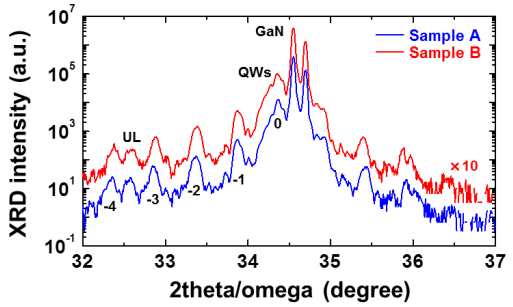

Fig. 2. 2θ–ω XRD scan spectra for samples A and B.

3. Experimental results, analysis, and discussion

In the case of GaInN/GaN QWs growth using the MOVPE, the impurity/defect incorporation into QWs drastically increases as the growth temperature lowers. Thus, a higher NRC density in yellow-red QWs compared to blue QWs is typically expected since the impurities/defects act

Optics EXPRESS

as NRCs in the QWs after incorporation by forming deep-levels in the forbidden gap [31,32]. That is, the growth temperature is one of the major factors determining the NRC density in the GaInN/GaN QWs. Recent deep-level optical spectroscopy and SSPC studies have revealed that the deep-level defects in the GaInN QWs are intensively distributed in two distinct energy levels in the forbidden gap: (i) E_{T1}, the deep-level defect located near the middle of the forbidden gap (typically corresponding to about $E_i - E_{T1} = 0.2{\sim}0.3$ eV; thus about $E_{T1} = E_c - 1.5$ eV for the $Ga_{0.70}In_{0.30}N$/GaN QWs in this study), and (ii) E_{T2}, the deep-level defects located above the valence band maximum (corresponding to about $E_{T2} = E_c - 2.0$ eV for the $Ga_{0.70}In_{0.30}N$/GaN QW in this study) [31–34]. To confirm the energy level of deep-level defects in the samples under investigation, the SSPC spectra were measured from 1.2 eV to 2.3 eV with 0.05 eV step at –3.1 V for sample A and –7.2 V for sample B, respectively. Here, the different reverse biases were applied to maintain the depletion width the same between the samples. The SSPC spectra were measured under broadband illumination of a 150 W xenon arc lamp (L2273, Hamamatsu Photonics Co., Japan) dispersed through a monochromator. The data was recorded after the increase in C (ΔC) was saturated. The experimental results are shown in Fig. 3(a), where arrows represent the onsets of deep-levels, found by significant changes in slope. From the photon energy of the onsets in Fig. 3(a), we can confirm that the energy levels of deep-level defects, i.e., E_{T1} and E_{T2}, were almost identical to each other and similar to the previous studies. [31–34]. Furthermore, for the samples in this study, we expect a lower density of NRCs in sample B compared to A, despite identical growth temperatures, since the pre-TMIn flow treatment of the QWs appeared to work well for suppression of defect/impurity incorporation (thus, we hypothesize that ΔC was measured lower in sample B.) [27]. To identify our hypothesis, we used PACV measurement, which is one of the useful means to quantitatively survey the defect/trap density (N_t) in the forbidden gap of a depletion layer, i.e., the QW active layer of the prepared samples [31–33]. The PACV curves can be obtained by measuring capacitance-voltage (C-V) curves under monochromatic sub-bandgap illumination. Under the illumination, the space-charge density increases because the charged-carriers are photo-excited from the deep-levels to the conduction band, resulting in the increase in C at a given V. Using this characteristic, the depth profile of N_t at a specific energy level across the QW active layer can be selectively surveyed by adjusting the applied reverse voltage and the photon energy of the monochromatic illumination. Armstrong *et al*. characterized the depletion width (DW, x) and N_t for the PACV curves mentioned above as [32,33]

$$\Delta V = \frac{q}{\varepsilon}\int_0^{x_d} xN_t(x)dx, \tag{1}$$

where q, ε, and x_d are the elementary charges, the semiconductor permittivity, and the DW at a given V, respectively. ΔV represents the additional voltage required to maintain a constant C (and therefore the same DW) [33]. Considering the result in Fig. 3(a), i.e., the almost identical onsets between the samples, the PACV curves in this study were measured under illuminations of 785 nm (~1.6 eV) and 594 nm (~2.1 eV) continuous-wave lasers (OBIS series, Coherent Inc., USA). That is to say, illuminations of 785 nm and 594 nm were adapted to photo-excite the charged-carriers only at E_{T1}, and both at E_{T1} and E_{T2}, respectively. We can investigate the defect profile at E_{T2} separately by subtracting ΔV from the 594 nm laser with the 785 nm laser. Figures 3(b) and (c) show the experimental results of the dark C-V (without the illumination) and PACV curves under the illumination of 594 and 785 nm lasers for samples A and B, respectively. The SSPC spectra and PACV curves were measured using a Keithley 4200A semiconductor parameter analyzer at a fixed modulation voltage of 30 mV and a fixed modulation frequency of 50 kHz to ensure data accuracy, i.e., the phase angles for PACV curves were closest to −90° under these conditions over the entire applied bias range. Before measuring the PACV curve and SSPC spectra, the sample was driven at +10 mA for 90 s to fill the defect sites with the

Optics EXPRESS

charged-carriers. In Figs. 3(b) and (c), the QWs are numbered, with QW1 closest to the n-type GaN, and DW decreased toward the EBL as the applied reverse bias decreased due to asymmetric depletion in GaInN-based junction semiconductors [35,36]. This is because the much higher acceptor (Mg) doping level in the p-type layer than the donor (Si) doping level in the n-type layer (about 25 folds in the samples under investigation) introduced the asymmetric expansion of depletion layer as the applied reverse bias increases. The insets are enlarged graphs around 0 V of the experimental data; here, ΔV_1 corresponds to the defect density at E_{T1} ($N_{t,1}$) and ΔV_2 corresponds to the defect density at E_{T2} ($N_{t,2}$), respectively. It is worth noting that three and two QWs were respectively depleted within the applied reverse bias range in samples A and B.

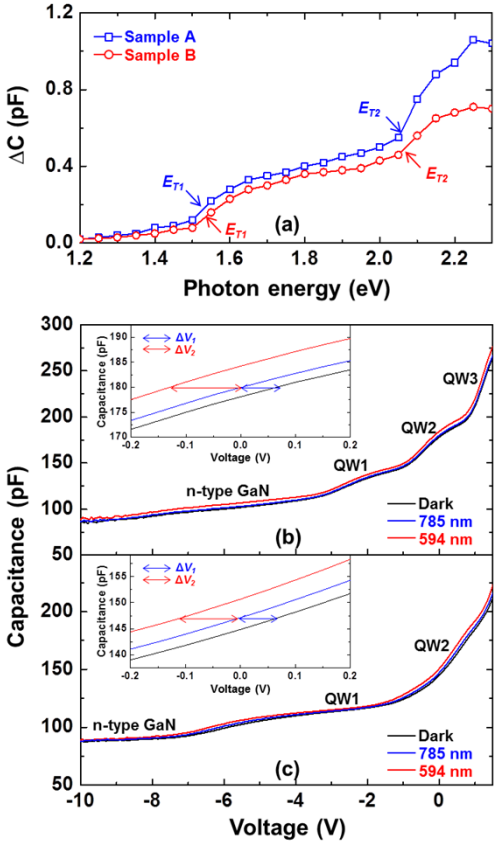

Fig. 3. (a) SSPC spectra from 1.2 eV to 2.3 eV of samples A and B. Therein, arrows represent the onsets of each deep-level, found by significant changes in slope. Experimental results of dark *C-V* (without the illumination) and PACV curves under the 785-nm and 594-nm continuous-wave laser illumination of samples (b) A and (c) B. Therein, QWs are numbered with QW1 being the closest to the n-type GaN. The insets are enlarged graphs around 0 V.

Combining the experimental results of ΔV_1 and ΔV_2 in Figs. 3(b) and (c) with Eq. (1), we can plot $N_{t,1}$ and $N_{t,2}$ for the depleted QWs of each sample. The results are shown in Fig. 4(a) and (b) for $N_{t,1}$ and $N_{t,2}$ of the samples A and B, respectively. For the sake of simplicity, we assumed that N_t is zero outside the QWs and x is zero at the EBL. The results exhibit that $N_{t,1}$ was comparable for both samples, whereas $N_{t,2}$ was remarkably decreased in sample B. These results indicate that the pre-TMIn flow treatment of the QWs was more effective at reducing $N_{t,2}$. Besides, $N_{t,1}$ seems to be distributed uniformly across the QWs. In contrast, $N_{t,2}$ seems to be drastically reduced from the QW1 to the EBL for both samples. It should be noted that the depth profile $N_{t,1}$ and $N_{t,2}$ of

Optics EXPRESS

the $Ga_{0.70}In_{0.30}N$/GaN QWs in this study (i.e., the QWs with high In content) are different from those of blue and near ultraviolet GaInN QWs (i.e., the QWs with low In content). Specifically, contrary to the result in Fig. 4, in the QWs with the low In content, the density of $N_{t,1}$ (i.e., the deep-level defect located near the middle of the forbidden gap) was higher than $N_{t,2}$, therefore $N_{t,1}$ plays a more significant role in forming the NRCs in blue and near ultraviolet GaInN QWs [31,34]. Such different defect characteristics raise the question about the factors limiting the IQE of the yellow-red emitting QWs.

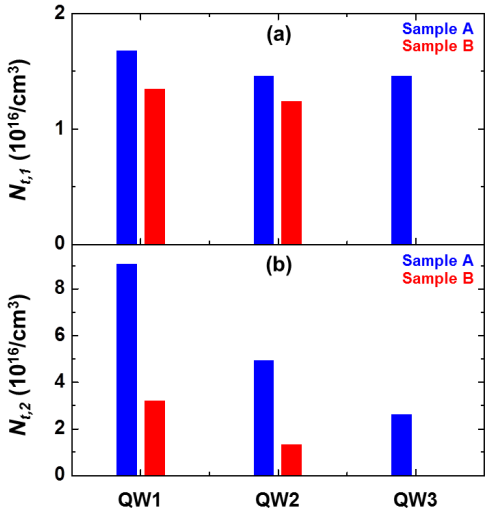

Fig. 4. Depth profiles of (a) $N_{t,1}$ and (b) $N_{t,2}$ for samples A (blue bars) and B (red bars) obtained by combining the experimental results of ΔV_1 and ΔV_2 in Fig. 3 with Eq. (1).

It was reported that V_{Ga}- and impurity-related complexes, e.g., V_{Ga}-donor complexes, carbon impurities, and V_{Ga}-impurity complexes, are one of the dominant sources for the deep-level transition in the GaInN QWs. Meanwhile, V_N-related defects, divacancies—comprising Ga and N vacancies and complexes (e.g., V_N, V_NV_{Ga}, V_N-carbon complexes, C_N, and C_NO_N impurity complexes)—are another dominant source for the deep-level transition in the GaInN QWs [37–40]. Here, we consider that the dominant source of $N_{t,1}$ and $N_{t,2}$ in the QWs would be different. It was reported that the incorporation of V_N-related defects/complexes into the QWs most likely originates via diffusion/penetration from the n-type GaN surface. Specifically, the V_N-related defects/complexes are segregated at the growth surface of the n-type GaN layer during high-temperature growth because of their low formation energy; they then incorporate into the GaInN/GaN QWs during low-temperature growth [27,40–43]. Thus, we speculate that the dominant source of $N_{t,2}$ is most likely V_N-related defects/complex since $N_{t,2}$ decreased exponentially from the QW1 to the QW3 in both samples —like a diffusion process, as exhibited in Fig. 4(b). Again, the decrease in $N_{t,2}$ from the QW closest to the n-side (QW1) to the QW far from the n-side (QW3) is believed to be originated that the type of $N_{t,2}$ is most likely the V_N-related defects/complexes and they were incorporated in the QWs via the diffusion process from the n-type GaN surface. During the diffusion process, most of them were preferentially incorporated into the QW closest to the n-side, and the rest contributed to the incorporation into the next QW because the V_N-related defects are easily incorporated with In atoms owing to their strong mutual affinity [33,41–43]. That is, $N_{t,2}$ can easily incorporate into the QWs with the high In content. For that reason, $N_{t,2}$ is predominant in the QW with the high In content, unlike the QWs with the low In content. In this viewpoint, the pre-TMIn flow treatment of the QWs can effectively suppress the incorporation of $N_{t,2}$ to the QWs because the atomic reaction between In

Optics EXPRESS

atoms and $N_{t,2}$ partially deactivate/neutralize them before incorporation into the QWs (therefore $N_{t,2}$ was measured lower in sample B) [27]. Consequently, only the density of $N_{t,2}$ was lower in sample B; however, other properties were the same for both samples thanks to the pre-TMIn flow treatment of the QWs.

In an effort to investigate the localization characteristics of the samples, we acquired top-view μ-CCD images of the 2-D EL emission distribution at driving currents of 1 μA (scanning area of 5×5 μm^2) and 10 μA (scanning area of 50×50 μm^2) for the samples using a high-resolution cooled CCD camera (PHEMOS-2000, Hamamatsu Co., Japan). The resultant images (Fig. 5) were acquired after cooling the CCD to ~223 K and processed to be normalized to each peak's EL intensity. Here, the driving currents of 1 μA in Figs. 5(a) and (b), and 10 μA in Figs. 5(c) and (d) correspond to the current densities of ~1.1 mA/cm^2 and ~11 mA/cm^2, respectively. The EL emissions appeared to be more localized in sample A, i.e., the spatial distribution of EL emission in sample B was more uniform compared to that of sample A for both scanning areas (i.e., driving currents). Typically, the localized dot-like emission is observable in GaInN/GaN QWs with the high In content because random alloy fluctuation during low-temperature growth creates In-rich regions. The charged-carriers are preferentially localized in the In-rich regions that act as the CLCs, and then recombine there [7,22,44]. For that reason, the EL emissions can be observed predominantly in the In-rich regions of QWs. Considering the results in Fig. 5, we can infer the more severe In clustering in sample A. Here, the different characteristics of In clustering between two samples can be attributed mainly to the $N_{t,2}$ as there were no differences between the samples other than $N_{t,2}$.

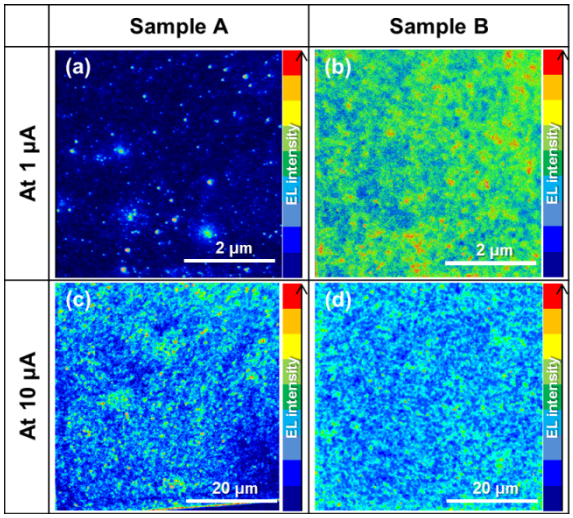

Fig. 5. 2–D μ-EL emission distribution images (top-view) of samples A and B obtained using a cooled CCD camera (a)-(b) at 1 μA (scanning area of 5×5 μm^2) and (c)-(d) at 10 μA (scanning area of 50×50 μm^2). All images are normalized to each peak's EL intensity.

Next, in an effort to investigate the role of the CLCs on device performance, we measured the electroluminescence (EL) spectra at a moderate driving current of 80 mA [Fig. 6(a)] and the power-weighted mean photon energy of EL spectra as a function of the driving current [Fig. 6(b)] using a spectrometer (AvaSpec-ULS2048, Avantes Co., USA) and a Keithley 2602 SourceMeter in the pulsed-current mode (pulse period = 100 μs and duty cycle = 1%). The pulsed-current mode was adopted to avoid self-heating effects. As depicted in Fig. 6(a), the EL spectrum was shifted to a longer wavelength, and its intensity was enhanced in sample B. Notably, a more dramatic blue-shift of the EL spectrum as driving current increases was observed in sample A, as

Optics EXPRESS

displayed in Fig. 6(b). Overall, the EL emission characteristics including the intensity and shift seem to be improved in sample B. The external quantum efficiency (EQE) and operating voltage of samples were measured using a Si photo-diode (S2281-04, Hamamatsu Co., Japan) under the pulsed-current driving conditions and plotted as a function of the driving current [Fig. 6(c)]. The results show that sample B had a higher EQE despite operating at a longer wavelength than sample A, and had a lower operating voltage. Here, the improved EQE can be attributed to the improved IQE since the structural impact was negligible between two samples, as shown in Fig. (2). Again, the different characteristics in EL emission and operating voltage between two samples in Figs. 6(a)–(c) can be attributed mainly to the different $N_{t,2}$ densities as mentioned above.

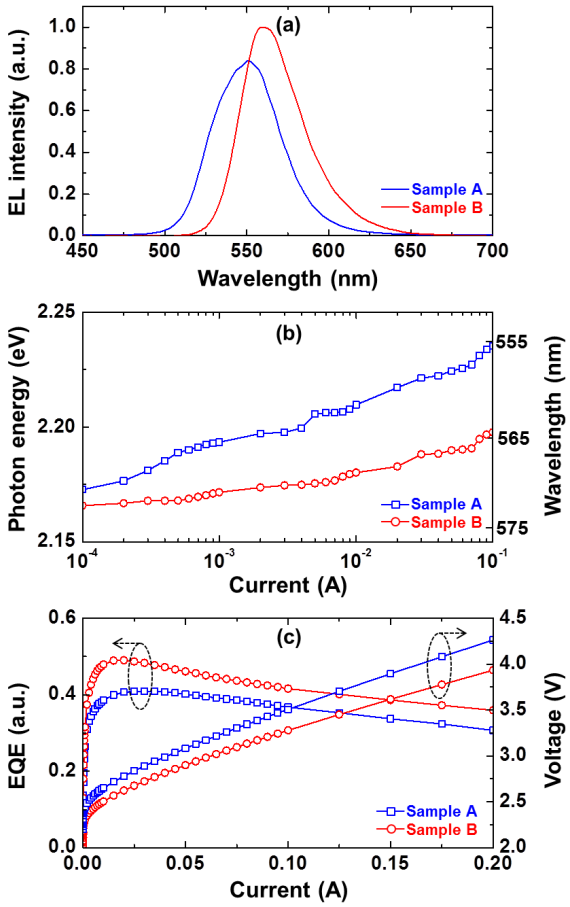

Fig. 6. Experimental results of (a) the EL spectra at a moderate driving current of 80 mA, (b) the power-weighted mean photon energy of EL spectra plotted as a function of the driving current on a semi-log scale, and (c) EQE and operating voltage plotted as a function of the driving current on a linear scale for samples A and B.

To explain the physical mechanism behind the experimental results in Figs. 5 and 6, we proposed the models along the in-plane direction of QW including $N_{t,2}$ distribution, In content, and carrier dynamics in Fig. 7(a)–(f).

First principles studies have figured out that the native defects, especially V_N-related defects/complexes, prefer to be situated close to their nearest neighbors in InN, forming vacancy clusters with a metallic-like bonding [45]. This means that the residual $N_{t,2}$ in the QWs tend

Optics EXPRESS

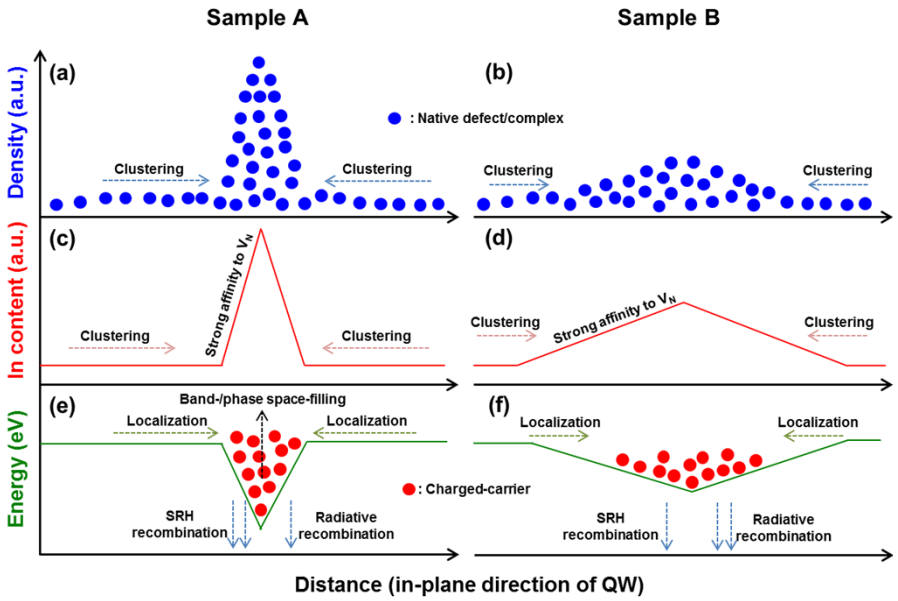

Fig. 7. Schematic illustration of proposed models of (a)–(b) the native defect/complex density, (c)–(d) In content, and (e)–(f) energy band diagram including charged-carrier and recombination processes along the in-plane direction of the QW for (a), (c), (e) sample A (b), (d), (f) and sample B, respectively.

to form the cluster since the type of $N_{t,2}$ was speculated to be most likely the V_N-related defects/complexes. Thus, the larger residual $N_{t,2}$ in sample A [recall Fig. 4(b)] introduced the more severe native defects/complexes cluster in the QWs [Figs. 7(a) and (b)]. Subsequently, as the native defects/complexes were spatially localized, the In-rich regions were formed at the native defects/complexes clusters due to their strong mutual affinity. In other words, the In-rich regions in the QWs were not only formed by the random alloy fluctuations, but also promoted by the native defects/complexes clusters—unlike blue QWs. For that reason, the more severe In clustering was expected in sample A due to the more severe native defects/complexes cluster [Figs. 7(c) and (d)]. When the device is forward biased, the charged-carriers are injected into the QWs; they preferentially occupy the In-rich regions (i.e., the CLCs) because of the nature of carrier relaxation. Thus, charged-carriers were expected to be localized in smaller CLCs more severely in sample A [Figs. 7(e) and (f)]. As the charged-carriers were spatially localized within the smaller CLCs in sample A, the EL emission was localized more severely in sample A, as displayed in Fig. 5. To be short, the CLCs in the QWs with the high In content were introduced by the native defect clustering, resulting in the localized EL emission.

Since the area that can be preferentially occupied by charged-carriers was greatly reduced in sample A, their pile-up in the CLCs rapidly increased as driving current increased [Figs. 7(e) and (f)]. Afterward, they move to higher energy states and recombine; this is typically known as the band-filling effect [35,46]. As a result, higher localization in sample A induces a more dramatic blue-shift of the EL spectrum [Figs. 6(a) and (b)]. It should be noted that the CLCs work as radiative recombination centers (RRCs) as well as NRCs since the CLCs creation in the QWs was promoted by the native defect clustering as mentioned above. Thus, the SRH recombination rate was expected to increase in sample A. Moreover, we expected the reduction of the radiative recombination rate in sample A since the charged-carrier pile-up in the 1-D quantum-dot like CLCs rapidly increased the hole-electron wave function mismatch in *k*-space; this is typically known as the phase-filling effect [22–24,47–49]. Consequently, the lower IQE of

Optics EXPRESS

sample A was the result of the higher localization simultaneously increasing the non-radiative SRH recombination rate and decreasing the radiative recombination rate. Another problem caused by the smaller CLCs is the additional potential drop. In detail, the pile-up of charged-carriers in the small CLCs induce a strong space-charge effect, i.e., the non-neutralized charged-carriers in an intrinsic active layer induce that the charge neutrality condition in the intrinsic active layer is no longer held, they thus act as uncompensated space-charges generating an electric field, which consequently increases electric potential energy to transport the charged-carrier [49–51]. Therefore, the higher operating voltage in sample A [Fig. 6(c)] was also physically caused by the higher localization of charged-carriers in the smaller CLCs.

4. Summary

In summary, this study aimed to understand the mechanism for creating CLCs in $Ga_{0.70}In_{0.30}N$/GaN QWs and examined their impacts on device performance. To this end, we compared two GaInN-based LED samples with and without TMIn flow-treated QWs. Here, the QWs were subjected to a pre-TMIn flow treatment to control the incorporation of defects/impurities in the QWs. Through the SSPC and PACV measurements and analysis, the pre-TMIn flow treatment of the QWs appeared to work well for the suppression of defect/impurity incorporation. Based on the experimental results and considerations, we showed that the CLC creation in $Ga_{0.70}In_{0.30}N$/GaN QWs is closely related to native defects/complexes, that is, the nature of native defects clustering and the strong affinity to In atoms were major factors behind the creation of CLCs in the QWs with the high In content. Unlike blue QWs with the low In content, the CLCs play a negative role in the QWs with high In content since they increase the non-radiative recombination rate, decrease in the radiative recombination rate, and increase the operating voltage simultaneously. We firmly believe that the analysis in this study can provide a new perspective on CLCs in yellow-red QWs.

Funding. Nano & Material Technology Development Program through the National Research Foundation of Korea funded by Ministry of Science and ICT, South Korea (2021M3D1A2048623).

Acknowledgments. The authors would like to thank Mr. Ryoto Fujiki, Prof. Motoaki Iwaya, Prof. Tetsuya Takeuchi, Prof. Satoshi Kamiyama, and Prof. Isamu Akasaki at Meijo and Nagoya University Japan, for experimental support, valuable discussion, and great guidance.

Disclosures. The authors declare no conflicts of interest.

Data availability. The data that support the findings of this study are available from the corresponding author upon reasonable request.

References

1. H. Amano, R. Collazo, and C. D. Santi, *et al.*, "The 2020 UV emitter roadmap," J. Phys. D: Appl. Phys. **53**(50), 503001 (2020).
2. Y. Huang, E.-L. Hsiang, M.-Y. Deng, and S.-T. Wu, "Mini-LED, Micro-LED and OLED displays: present status and future perspectives," Light: Sci. Appl. **9**(1), 105 (2020).
3. K. Ding, V. Avrutin, N. Izyumskaya, Ü Özgür, and H. Morkoç, "Micro-LEDs, a Manufacturability Perspective," Appl. Sci. **9**(6), 1206 (2019).
4. P. J. Parbrook, B. Corbett, J. Han, T.-Y. Seong, and H. Amano, "Micro-Light Emitting Diode: From Chips to Applications," Laser Photonics Rev. **15**(5), 2000133 (2021).
5. I. Akasaki, "Nobel Lecture: Fascinated journeys into blue light," Rev. Mod. Phys. **87**(4), 1119–1131 (2015).
6. H. Amano, "Nobel Lecture: Growth of GaN on sapphire via low-temperature deposited buffer layer and realization of p-type GaN by Mg doping followed by low-energy electron beam irradiation," Rev. Mod. Phys. **87**(4), 1133–1138 (2015).
7. C. Tessarek, S. Figge, T. Aschenbrenner, S. Bley, A. Rosenauer, M. Seyfried, J. Kalden, K. Sebald, J. Gutowski, and D. Hommel, "Strong phase separation of strained $In_xGa_{1-x}N$ layers due to spinodal and binodal decomposition: Formation of stable quantum dots," Phys. Rev. B **83**(11), 115316 (2011).
8. S. Nakamura, "Nobel Lecture: Background story of the invention of efficient blue InGaN light emitting diodes," Rev. Mod. Phys. **87**(4), 1139–1151 (2015).

Optics EXPRESS

9. D.-P. Han, K. Yamamoto, S. Ishimoto, M. Iwaya, T. Takeuchi, S. Kamiyama, and I. Akasaki, "Determination of internal quantum efficiency in GaInN-based light-emitting diode under electrical injection: carrier recombination dynamics analysis," Appl. Phys. Express **12**(3), 032006 (2019).
10. M. Usman, M. Munsif, U. Mushtaq, A.-R. Anwar, and N. Muhammad, "Green gap in GaN-based light-emitting diodes: in perspective," Crit. Rev. Solid State Mater. Sci. **46**(5), 450–467 (2021).
11. S. Roy, S. M. T. Ahsan, A. H. Howlader, D. Kundu, Md. S. M. Boby, Md. R. Islam, S. A. Khan, S. Dhar, and Md. A. Hossain, "Comparative investigation into polarization field-dependent internal quantum efficiency of semipolar InGaN green light-emitting diodes: A strategy to mitigate green gap phenomenon," Mater. Today Commun. **31**, 103705 (2022).
12. Q. Zhou, M. Xu, and H. Wang, "Internal quantum efficiency improvement of InGaN/GaN multiple quantum well green light-emitting diodes," Opto-Electron. Rev. **24**(1), 1–9 (2016).
13. S. Saito, R. Hashimoto, J. Hwang, and S. Nunoue, "InGaN Light-Emitting Diodes on c-Face Sapphire Substrates in Green Gap Spectral Range," Appl. Phys. Express **6**(11), 111004 (2013).
14. R. Takahashi, R. Fujiki, K. Hozo, R. Hiramatsu, M. Matsukura, T. Kojima, D.-P. Han, M. Iwaya, T. Takeuchi, and S. Kamiyama, "Improvement of 650-nm red-emitting $GaIn_{0.17}N/GaIn_{0.38}N$ multiple quantum wells on $ScAlMgO_4$ (2022) substrate by suppressing impurity diffusion/penetration," Appl. Phys. Lett. **120**(14), 142102 (2022).
15. D. Iida, K. Niwa, S. Kamiyama, and K. Ohkawa, "Demonstration of InGaN-based orange LEDs with hybrid multiple-quantum-wells structure," Appl. Phys. Express **9**(11), 111003 (2016).
16. Y. Zhao, S. H. Oh, F. Wu, Y. Kawaguchi, S. Tanaka, K. Fujito, J. S. Speck, S. P. DenBaars, and S. Nakamura, "Green Semipolar () InGaN Light-Emitting Diodes with Small Wavelength Shift and Narrow Spectral Linewidth," Appl. Phys. Express **6**, 062102 (2013).
17. J.-I. Hwang, R. Hashimoto, S. Saito, and S. Nunoue, "Development of InGaN-based red LED grown on (2014) polar surface," Appl. Phys. Express **7**(7), 071003 (2014).
18. S. Ishimoto, D.-P. Han, K. Yamamoto, S. Kamiyama, T. Takeuchi, M. Iwaya, and I. Akasaki, "Improvement of emission efficiency with a sputtered AlN buffer layer in GaInN-based green light-emitting diodes," Jpn. J. Appl. Phys. **58**(SC), SC1040 (2019).
19. I.-K. Park, M.-K. Kwon, J.-O. Kim, S.-B. Seo, J.-Y. Kim, J.-H. Lim, and S.-J. Park, "Green light-emitting diodes with self-assembled In-rich InGaN quantum dots," Appl. Phys. Lett. **91**(13), 133105 (2007).
20. S. Kamiyama, W. Lu, T. Takeuchi, M. Iwaya, and I. Akasaki, "Growth and Characterization of Core-Shell Structures Consisting of GaN Nanowire Core and GaInN/GaN Multi-Quantum Shell," ECS J. Solid State Sci. Technol. **9**(1), 015007 (2020).
21. P. Li, H. Li, H. Zhang, Y. Yang, M. S. Wong, C. Lynsky, M. Iza, M. J. Gordon, J. S. Speck, S. Nakamura, and S. P. DenBaars, "Red InGaN micro-light-emitting diodes (>620 nm) with a peak external quantum efficiency of 4.5% using an epitaxial tunnel junction contact," Appl. Phys. Lett. **120**(12), 121102 (2022).
22. S. Y. Karpov, "Carrier localization in InGaN by composition fluctuations: implication to the "green gap"," Photonics Res. **5**(2), A7–A12 (2017).
23. A. David, N. G. Young, and M. D. Craven, "Many-Body Effects in Strongly Disordered III-Nitride Quantum Wells: Interplay Between Carrier Localization and Coulomb Interaction," Phys. Rev. Appl. **12**(4), 044059 (2019).
24. M. A. D. Maur, A. Pecchia, G. Penazzi, W. Rodrigues, and A. D. Carlo, "Efficiency Drop in Green InGaN = GaN Light Emitting Diodes: The Role of Random Alloy Fluctuations," Phys. Rev. Lett. **116**(2), 027401 (2016).
25. A. Kaneta, M. Funato, and Y. Kawakami, "Nanoscopic recombination processes in InGaN/GaN quantum wells emitting violet, blue, and green spectra," Phys. Rev. B **78**(12), 125317 (2008).
26. S. F. Chichibu, A. Uedono, T. Onuma, B. A. Haskell, A. Chakraborty, T. Koyama, P. T. Fini, S. Keller, S. P. Denbaars, J. S. Speck, U. K. Mishra, S. Nakamura, S. Yamaguchi, S. Kamiyama, H. Amano, I. Akasaki, J. Han, and T. Sota, "Origin of defect-insensitive emission probability in In-containing (Al,In,Ga)N alloy semiconductors," Nat. Mater. **5**(10), 810–816 (2006).
27. D.-P. Han, M. Iwaya, T. Takeuchi, and S. Kamiyama, "Pre-trimethylindium Flow Treatment of GaInN/GaN Quantum Wells to Suppress Surface Defect Incorporation and Improve Efficiency," ACS Appl. Mater. Interfaces **14**(22), 26264–26270 (2022).
28. T. Sugiyama, D. Iida, T. Yasuda, M. Iwaya, T. Takeuchi, S. Kamiyama, and I. Akasaki, "Extremely Low-Resistivity and High-Carrier-Concentration Si-Doped $Al_{0.05}Ga_{0.95}N$," Appl. Phys. Express **6**(12), 121002 (2013).
29. R. Fujiki, R. Takahashi, R. Hiramatsu, K. Hozo, D.-P. Han, M. Iwaya, T. Takeuchi, and S. Kamiyama, "Hydrogen *in-situ* etching of GaN surface to reduce non-radiative recombination centers in 510-nm GaInN/GaN quantum-wells," J. Cryst. Growth **593**, 126751 (2022).
30. M. A. Moram and M. E. Vickers, "X-ray diffraction of III-nitrides," Rep. Prog. Phys. **72**(3), 036502 (2009).
31. A. Armstrong, T. A. Henry, D. D. Koleske, M. H. Crawford, and S. R. Lee, "Quantitative and depth-resolved deep level defect distributions in InGaN/GaN light emitting diodes," Opt. Express **20**(S6), A812–A821 (2012).
32. A. M. Armstrong, M. H. Crawford, and D. D. Koleske, "Contribution of deep-level defects to decreasing radiative efficiency of InGaN/GaN quantum wells with increasing emission wavelength," Appl. Phys. Express **7**(3), 032101 (2014).
33. A. Armstrong, T. A. Henry, D. D. Koleske, M. H. Crawford, K. R. Westlake, and S. R. Lee, "Dependence of radiative efficiency and deep level defect incorporation on threading dislocation density for InGaN/GaN light emitting diodes," Appl. Phys. Lett. **101**(16), 162102 (2012).

Optics EXPRESS

34. F. Piva, C. De Santi, A. Caria, C. Haller, J. F. Carlin, M. Mosca, G. Meneghesso, E. Zanoni, N. Grandjean, and M. Meneghini, "Defect incorporation in In-containing layers and quantum wells: experimental analysis via deep level profiling and optical spectroscopy," J. Phys. D: Appl. Phys. **54**(2), 025108 (2021).
35. D.-P. Han, J.-I. Shim, D.-S. Shin, and K.-S. Kim, "Effects of unbalanced carrier injection on the performance characteristics of InGaN light-emitting diodes," Appl. Phys. Express **9**(8), 081002 (2016).
36. T.-S. Kim, B.-J. Ahn, Y. Dong, K.-N. Park, J.-G. Lee, Y. Moon, H.-K. Yuh, S.-C. Choi, J.-H. Lee, S.-K. Hong, and J.-H. Song, "Well-to-well non-uniformity in InGaN/GaN multiple quantum wells characterized by capacitance-voltage measurement with additional laser illumination," Appl. Phys. Lett. **100**(7), 071910 (2012).
37. M. A. Reshchikov, D. O. Demchenko, A. Usikov, H. Helava, and Y. Makarov, "Carbon defects as sources of the green and yellow luminescence bands in undoped GaN," Phys. Rev. B **90**(23), 235203 (2014).
38. D.-P. Han, R. Fujiki, R. Takahashi, Y. Ueshima, S. Ueda, W. Lu, M. Iwaya, T. Takeuchi, S. Kamiyama, and I. Akasaki, "n-type GaN surface etched green light-emitting diode to reduce non-radiative recombination centers," Appl. Phys. Lett. **118**(2), 021102 (2021).
39. J. Buckeridge, C. R. A. Catlow, D. O. Scanlon, T. W. Keal, P. Sherwood, M. Miskufova, A. Walsh, S. M. Woodley, and A. A. Sokol, "Determination of the nitrogen vacancy as a shallow compensating center in GaN doped with divalent metals," Phys. Rev. Lett. **114**(1), 016405 (2015).
40. Y. Chen, C. Haller, W. Liu, S. Y. Karpov, J.-F. Carlin, and N. Grandjean, "GaN buffer growth temperature and efficiency of InGaN/GaN quantum wells: The critical role of nitrogen vacancies at the GaN surface," Appl. Phys. Lett. **118**(11), 111102 (2021).
41. C. Haller, J.-F. Carlin, G. Jacopin, D. Martin, R. Butté, and N. Grandjean, "Burying non-radiative defects in InGaN underlayer to increase InGaN/GaN quantum well efficiency," Appl. Phys. Lett. **111**(26), 262101 (2017).
42. D.-P. Han, S. Ishimoto, R. Mano, W. Lu, M. Iwaya, T. Takeuchi, S. Kamiyama, and I. Akasaki, "Efficiency Enhancement Mechanism of an Underlying Layer in GaInN-Based Green Light–Emitting Diodes," Phys. Status Solidi A **217**(7), 1900713 (2020).
43. C. Haller, J.-F. Carlin, G. Jacopin, M. Mosca, M. D. Rossell, R. Erni, and N. Grandjean, "InAlN underlayer for near ultraviolet InGaN based light emitting diodes," Appl. Phys. Express **12**(3), 034002 (2019).
44. Y. Kawakami, Y. Narukawa, K. Sawada, S. Saijyo, S. Fujita, S. Fujita, and S. Nakamura, "Recombination dynamics of localized excitons in self-formed InGaN quantum dots," Mater. Sci. Eng. B. **50**(1-3), 256–263 (1997).
45. X. M. Duan and C. Stampfl, "Nitrogen vacancies in InN: Vacancy clustering and metallic bonding from first principles," Phys. Rev. B **77**(11), 115207 (2008).
46. D.-P. Han, C.-H. Oh, D.-S. Shin, J.-I. Shim, M. Iwaya, T. Takeuchi, S. Kamiyama, and I. Akasaki, "Thermodynamic analysis of GaInN-based light-emitting diodes operated by quasi-resonant optical excitation," J. Appl. Phys. **128**(12), 123103 (2020).
47. A. David and M. J. Grundmann, "Droop in InGaN light-emitting diodes: A differential carrier lifetime analysis," Appl. Phys. Lett. **96**(10), 103504 (2010).
48. L. Wang, C. Lu, J. Lu, L. Liu, N. Liu, Y. Chen, Y. Zhang, E. Gu, and X. Hu, "Influence of carrier screening and band filling effects on efficiency droop of InGaN light emitting diodes," Opt. Express **19**(15), 14182–14187 (2011).
49. D.-P. Han, H. Kim, J.-I. Shim, D.-S. Shin, and K.-S. Kim, "Influence of carrier overflow on the forward-voltage characteristics of InGaN-based light-emitting diodes," Appl. Phys. Lett. **105**(19), 191114 (2014).
50. S. M. Sze and K. K. Ng, *Physics of Semiconductor Devices*, 3rd ed. (Wiley, Hoboken, NJ, USA, 2007) chapter. 1.
51. D.-P. Han, D.-S. Shin, J.-I. Shim, S. Kamiyama, T. Takeuchi, M. Iwaya, and I. Akasaki, "Modified Shockley Equation for GaInN-based Light-emitting Diodes: Origin of the Power-efficiency Degradation Under High Current Injection," IEEE J. Quantum Electron. **55**(4), 1–11 (2019).